



HAL
open science

Hierarchical Model Predictive Control to Coordinate a Vehicle-to-Grid System Coupled to Building Microgrids

Daniela Yassuda Yamashita, Ionel Vechiu, Jean-Paul Gaubert, Samuel Jupin

► **To cite this version:**

Daniela Yassuda Yamashita, Ionel Vechiu, Jean-Paul Gaubert, Samuel Jupin. Hierarchical Model Predictive Control to Coordinate a Vehicle-to-Grid System Coupled to Building Microgrids. IEEE Transactions on Industry Applications, 2022, pp.1-10. 10.1109/TIA.2022.3215978 . hal-03916925

HAL Id: hal-03916925

<https://hal.science/hal-03916925v1>

Submitted on 31 Dec 2022

HAL is a multi-disciplinary open access archive for the deposit and dissemination of scientific research documents, whether they are published or not. The documents may come from teaching and research institutions in France or abroad, or from public or private research centers.

L'archive ouverte pluridisciplinaire **HAL**, est destinée au dépôt et à la diffusion de documents scientifiques de niveau recherche, publiés ou non, émanant des établissements d'enseignement et de recherche français ou étrangers, des laboratoires publics ou privés.

Hierarchical Model Predictive Control to Coordinate a Vehicle-to-Grid System Coupled to Building Microgrids

Daniela Yassuda Yamashita, Ionel Vechiu, *Senior Member, IEEE*, Jean-Paul Gaubert, *Member, IEEE*, Samuel Jupin

Abstract— Aiming to take full advantage of Electric Vehicles' (EVs) batteries, this paper proposes a two-level hierarchical model predictive controller coupled with an innovative charging-discharging scheduler for EVs in Building Microgrids (BMGs). This paper provides a complete framework for the design of this control structure and analyses its performance regarding the state of charge of the EVs at departure time, the self-consumption rate, and the coverage rate, considering a residential BMG equipped with photovoltaic panels and static Li-ion batteries. The results and performance of the proposed control architecture are compared to two other solutions: a hierarchical predictive controller with no scheduler and a rule-based algorithm. A technological and economical study is also performed considering variables such as the dimension of the EV's park, the price of energy, the cost of maintenance, the possibility to discharge or not into the grid, and the execution time of the control architecture. The simulation results conducted in MATLAB Simulink demonstrated that the proposed control structure ensures the full charging of all vehicles at departure time while also improving the self-consumption rate of the BMG with a relatively low stress on the needed computation capacities, even when considering a large fleet of vehicles.

Keywords—Model Predictive Control, Electric Vehicles, Building microgrid, self-consumption, economic analysis

I. INTRODUCTION

WITH the fast electrification in the transportation sector, Electric Vehicles (EVs) play a critical role in meeting the environmental goals to address climate change [1]. However, without appropriate coordination of EV charging, the sharp increase of EV fleets [2] can introduce harmful effects on the grid stability, such as overload of transformers and power quality issues [3]–[5]. To adapt the current grid to this new paradigm, EVs in the bidirectional Vehicle-to-Grid (V2G) configuration have emerged as a promising strategy to reduce the negative effects of EV surge [6]–[8]. Variations on this approach also exist, such as Vehicle to Building [9], [10] and Vehicle to Home [11]. This is because V2G technology enables EVs to be employed as both a flexible load and an Energy Storage System (ESS) [12].

Consequently, while parked, EV's batteries can provide some grid services to assist the integration of Renewable Energy Sources (RES) into the electrical grid that struggles with volatility in the power imbalance. EVs' batteries can be discharged to supply the local demand and can be charged to avoid the injection of RES energy surplus. Particularly, since EVs are parked for more than 90% of their lifetime, their batteries can be coupled to buildings' parking lots equipped with RES such as roof-top photovoltaic (PV) panels [13]. This grid topology – known as Building Microgrid (BMG) – facilitates EVs' owners to charge their vehicles' batteries with clean energy while at the same time reducing the

drawbacks created by unpredictable RES energy generation. Nonetheless, the design of a Building Energy Management System (BEMS) is required to properly coordinate the charging-discharging of EVs to improve the BMG's PV self-consumption and assure that all EVs are completely charged before their departure time [3].

In the literature, there are many strategies to coordinate the charging-discharging of EVs to promote PV self-consumption in buildings [9], [11], [14]–[16]. To assure that all EVs are fully charged and to maximise the PV self-consumption, the BEMS are usually divided twofold [6], [8]: a central unit to optimise the BMG power flow, and a real-time module to charge and discharge each EV according to a priority order [17]. However, the aleatory disconnection of EVs is hardly taken into account. In fact, a variety of algorithms incorporating machine learning and other prediction techniques are emerging to be added to the main energy management system to predict the availability of the EVs [15], [18]. Additionally, when dealing with large EV fleets, the computation burden is the main issue of power flow optimisation [3], [6], limiting the BMG power flow to be optimised only once a day. Alternatively, simple on-board strategies to EVs' power allocation exist [19], but they consider neither prediction data nor uncertainty in EVs' disconnection nor the use of another type of ESS. These solutions tackle complex micro-grids with a low computational effort, but they cannot handle their stochastic nature, therefore leading to non-optimal solutions.

Aiming at maximising PV self-consumption in BMG under stochasticity in prediction data, a two-level Model Predictive Controller (MPC) empowered with a light Electric Vehicle Power Allocation (EVPA) module was designed. Contrary to many studies [6], [7], the innovation of the proposed controller is that no parameter needs to be tuned to maximise the self-consumption rate and guarantee the full charging of EV fleets. The capabilities and robustness of the proposed hierarchical controller were assessed through simulations in MATLAB Simulink of a real-sized residential BMG equipped with PV, Li-ion batteries, and an EV parking with 4, 20, or 40 vehicles. Furthermore, this paper quantifies the additional degradation rate of EVs' batteries when they are discharged to supply the building energy demand and identifies a type of remuneration to foster EVs' owners to authorise using their EVs' batteries to promote self-consumption in BMGs. As extension of the authors' previous work [20], a sensitivity analysis on the electricity price and EV batteries price is conducted in order to identify the prices that would be economically advantageous to discharge the EVs batteries on behalf of the building energy demand. A complete economic and energetic study was led on these topics applied to the specific case study of the residential building. The results show two major conclusions: first, the

algorithm proposed and the suggested association of centralized units of control around the main MPC controller is efficient and behaves better than the all-in-one structure often presented in BEMS [6]–[8], [19]. Second, the choice of a residential building with intermittent solar power is not the most optimal one. In fact, a building where EVs park during the day would be much more remarkable when it comes to studying the interests of combining EVs to BMS.

The remainder of this paper is structured as follows. Section II presents the BMG understudy and the design of the hierarchical MPC. Section III details the proposed EVPA algorithm by highlighting its interaction with the two-level MPC. Section IV presents the simulation results with discussions over the system performance, comparing three different control structures with each other, considering the total grid energy exchange, building energy cost, and final EV users' interests. Finally, Section V concludes the paper with a discussion over the main results.

II. HIERARCHICAL MODEL PREDICTIVE CONTROLLER

As shown in Fig. 1, the BMG counts on static Li-ion batteries and a parking with up to N_{EV} EVs to supply its local demand as much as possible with PV energy generated locally. The proposed hierarchical BEMS – designed in C++ language – is composed of three control levels, namely: Economic MPC (EMPC), Tracking MPC (TMPC), and EVPA. Considering the prediction data of fluctuations in the internal power imbalance, the EMPC determines State-of-Charge (SoC) references of stationary batteries ($SoC_{bat,k}^{ref}$) and the references for EV parking stored energy ($E_{EV,k}^{ref}$) for each hour k . Therefore, the time discretization (T_s^{EMPC}) of EMPC is one hour. Before optimizing its cost function (1), the EMPC considers the most recent data predictions concerning the building power imbalance, and the state of charge of static Li-ion batteries and of the EV parking to calculate optimal setpoints for each ESS. These references are determined through the optimisation of the cost function defined in (1) using Mixed Integer Linear Programming of CPLEX framework.

$$\min_{SoC_{bat}^{ref}, E_{EV}^{ref}} \sum_{k=1}^{48h} |E_{grid,k}^{import}| + |E_{grid,k}^{export}| \quad (1)$$

s.t.: Eq.(5) – (16)

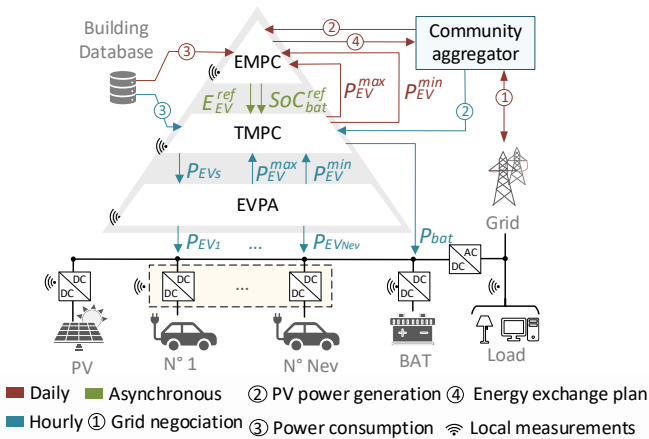


Fig. 1: Hierarchical building energy management system.

With this formulation, the BMG uses its ESS to maximise the PV self-consumption (τ_{sc}) and coverage (τ_c) rates defined by (2) and illustrated in Fig. 2, avoiding importing ($E_{grid,k}^{import}$) and exporting energy ($E_{grid,k}^{export}$). It minimizes the grid energy exchange by defining the setpoints for the batteries SoC and EV energy stored for the next 48 hours. The EMPC is an asynchronous control unit updated every midnight or when the gap between the expected grid exchange calculated by the EMPC internal models and the real one measured by the smart meter is higher than a pre-defined threshold (i.e. 7%). The errors in the EMPC's prediction states can come from either stochasticity in the power imbalance, imprecisions in the ESS's internal model, or unexpected EVs disconnection. The horizon of the EMPC is 48 hours ahead to consider the daily PV power fluctuations and avoid depleting the static Li-ion battery. Since the Li-ion batteries were sized to be completed charged and discharged during a day to avoid wasting energy due to self-discharging [21], the daily optimization of (1) will prevent the BMG from ending the day with static batteries completely discharged.

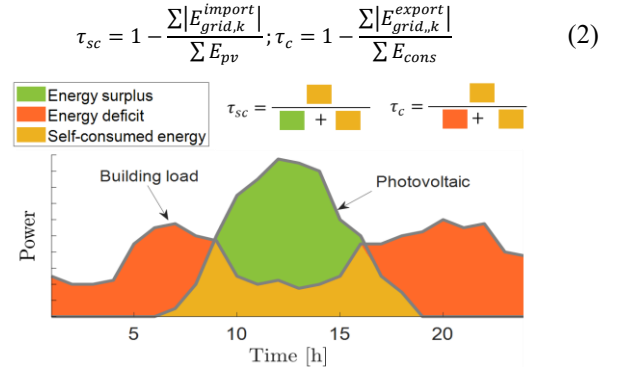


Fig. 2: Definition of self-consumption and coverage rate for a building microgrid.

Meanwhile, TMPC follows SoC_{bat}^{ref} and E_{EV}^{ref} determined by the EMPC. It calculates the power references for batteries (P_{BAT}^{ch} and P_{BAT}^{dis}) and for the entire EV parking (P_{EVs}^{ch} and P_{EVs}^{dis}) based on the updated prediction data and SoC measurements. Therefore, every hour, TMPC minimizes the error between the actual energy stored in ESSs and the EMPC setpoints, as defined in (4). The tracking of the stored energy in the EV parking and the SoC of Li-ion batteries is implemented within a horizon of 6 hours ahead to reduce the required computation time, while considering reliable prediction data of the building power imbalance ($P_{pv} - P_{cons}$). Therefore, before optimising (3), TMPC updates the SoC of Li-ion Batteries, the energy stored in the EV park with last data measurements. Additionally, the cost function expressed in (4) is normalised to make the error of each reference tracking between 0 and 1 by dividing each tracking error by its maximum values ($E_{EV,k}^{max}$ and SoC_{bat}^{max}). This normalization is important to make it independent of manually adjustable parameters, as in [6]. Additionally, aiming to give more importance to the instantaneous references than the upcoming references, the quadratic errors are multiplied by the term $(N_h^{TMPC} - k - 1)^2$, where N_h is the TMPC horizon and k is the time within the horizon window.

$$\min_{P_{BAT}^{ch,dis}, P_{EVs}^{ch,dis}} \sum_{k=1}^{N_h=6h} \underbrace{\left(\frac{N_h - k - 1}{SoC_{bat}^{max}} \right)^2 (SoC_{bat}^{ref} - SoC_{bat,k})^2}_{\text{Li-ion Batteries SoC tracking}} + \underbrace{\left(\frac{N_h - k - 1}{E_{EV,k}^{max}} \right)^2 (E_{EV}^{ref} - E_{EV,k})^2}_{\text{Electric Vehicle SoC tracking}} \quad (4)$$

s.t.: Eq.(5) – (16)

Both MPC objective functions have the same constraints to keep the safe operation of ESSs and respect the grid code for small prosumers in France [22]. In the first place, both MPCs must assure the energy balance by considering the equality constraint defined in (5), in which T_s is the time discretisation of the MPCs. The energy exchange between the external grid and the BMG has to be lower than the maximum supported by the infrastructure (E_{grid}^{max}). This limitation is modelled through the constraint expressed in (6). Furthermore, the charging and discharging of EV parking are limited by the maximum power rate of the aggregation of EVs (P_{EV}^{maxCh} and P_{EV}^{maxDis}), as defined in (7) and (8). The maximum power rate of EV parking is a variable that is updated by the EVPA module every hour.

To avoid taking advantages from fluctuations of electricity price, stationary batteries can be charged only with PV power surplus ($P_{cons} \leq P_{pv}$) as specified in (9). Meanwhile, they can only be discharged to supply the local power demand (P_{cons}) or charge EVs ($P_{EV,k}^{ch}$), as expressed in (10). Additionally, the power setpoint of Li-ion batteries are limited to their maximum power rate (P_{bat}^{maxDis} and P_{bat}^{maxCh}) specified in their datasheet. The Boolean variables δ_{EV}^{ch} or δ_{bat}^{ch} (i.e. δ_{EV}^{dis} or δ_{bat}^{dis}) are worth 1 when the ESS is charging (i.e. discharging); and 0 otherwise. Therefore, equation (11) avoids the controller charging and discharging each ESS simultaneously.

$$(P_{bat,k}^{ch} + P_{bat,k}^{dis} + P_{EVpark,k}^{ch} + P_{EVpark,k}^{dis} + P_{PV} - P_{cons}) \cdot T_s = E_{grid,k}^{import} + E_{grid,k}^{export} \quad (5)$$

$$\left| E_{grid,k}^{import} \right| \leq E_{grid}^{max}, \left| E_{grid,k}^{export} \right| \leq E_{grid}^{max} \quad (6)$$

$$P_{EV,k}^{maxCh} \delta_{EV,k}^{ch} \leq P_{EVpark,k}^{ch} \leq 0 \quad (7)$$

$$0 \leq P_{EVpark,k}^{dis} \leq P_{EV,k}^{maxDis} \delta_{EV,k}^{dis} \quad (8)$$

$$\min(P_{bat}^{maxCh} \cdot \delta_{bat,k}^{ch}; -P_{pv} + P_{cons}) \leq P_{bat,k}^{ch} \leq 0 \quad (9)$$

$$0 \leq P_{bat,k}^{ch} \leq \min(P_{bat}^{maxDis} \cdot \delta_{bat,k}^{dis}; P_{pv} - P_{cons} - P_{EV,k}^{ch}) \quad (10)$$

$$0 \leq \delta_{EV,k}^{ch} + \delta_{EV,k}^{dis} \leq 1; 0 \leq \delta_{bat,k}^{ch} + \delta_{bat,k}^{dis} \leq 1 \quad (11)$$

The link between battery power and its SoC is defined by the linear equation (12), where the Q_{nom}^{bat} is the batteries nominal capacity in Ah, v_{nom}^{bat} is the batteries nominal voltage, and η_{ch}^{bat} and η_{dis}^{bat} are the Li-ion batteries efficiency when the batteries are charging or discharging, respectively.

$$SoC_{k+1}^{bat} = SoC_k^{bat} + \frac{\eta_{ch}^{bat} T_s}{v_{nom}^{bat} \cdot Q_{nom}^{bat}} \cdot P_{bat,k}^{ch} + \frac{T_s}{v_{nom}^{bat} \cdot Q_{nom}^{bat} \eta_{dis}^{bat}} \cdot P_{bat,k}^{dis} \quad (12)$$

Remarkably, as in [7], to reduce computation burden, the two MPCs in cascade estimate the total energy stored in the aggregation of EVs ($E_{EV,k}$) rather than individual EVs. Therefore, only two inequalities constraints are embedded in the MPCs formulation to limit the EV parking SoC, as expressed in (13). In this equation, Q_{EV}^{nom} is the nominal capacity of an EV, $\bar{v}_{EV,k}$ is the average voltage of EVs connected at instant k , and η_{dis} and η_{ch} are the batteries discharging and charging efficiency.

$$E_{EV,k}^{min} = Q_{EV}^{nom} \cdot SoC_{EV}^{min} \cdot n_{EV,k} \leq E_{EV,k} - \frac{\eta_{ch} T_s}{\bar{v}_{EV,k}} P_{EV,k}^{ch} - \frac{T_s}{\bar{v}_{EV,k} \eta_{dis}} P_{EV,k}^{dis} + E_k^{arr} - E_k^{dep} \quad (13)$$

$$\leq Q_{EV}^{nom} \cdot SoC_{EV}^{max} \cdot n_{EV,k} = E_{EV,k}^{max}$$

To assure that all EVs are charged with the request SoC ($SoC^{target} = 80\%$) before their scheduled departure, EMPC and TMPC modify their SoC boundaries (SoC_{EV}^{min} and SoC_{EV}^{max}) to force both to be 80% when any EV is planning to disconnect to the BMG. In other words, the maximum boundary (SoC_{EV}^{max}) is always equal to 80%, whereas the minimum boundary (SoC_{EV}^{min}) is adjusted following equation (14), where n_k^{dep} is the number of EVs that are going to disconnect at hour k .

$$SoC_{EV}^{min} = \begin{cases} 20\%, & \text{if } n_k^{dep} = 0 \\ SoC_{EV}^{max}, & \text{otherwise} \end{cases} \quad (14)$$

Notably, in equation (13), the stochastic arrival and departure of EVs are considered through the variables E_k^{arr} and E_k^{dep} , representing the energy arrived with new EVs connection (E_k^{arr}) and the energy departure with EVs when they are disconnected (E_k^{dep}). Calculated through equations (15) and (16), E_k^{arr} and E_k^{dep} are estimated based on the total number of EVs plugged ($n_{EV,k}$), EVs departures (n_k^{dep}) and EVs arrivals (n_k^{arr}).

$$E_k^{arr} = n_k^{arr} \cdot Q_{EV}^{nom} \cdot \widehat{SoC}_{EVs,k}^{arr} \quad (15)$$

$$E_k^{dep} = n_k^{dep} \cdot E_{EV,k} / n_{EV,k} \quad (16)$$

These three values can be easily calculated using a simple EV schedule table based only on the current number of EVs connected, the next EV connection, and the disconnection time inputted by EVs' owners. Nevertheless, this mechanism can be improved by including an analysis of EV's behaviour, as proposed in [23]. The EV arrival energy formulation (equation (15)) considers that all EVs have the same nominal capacity (Q_{EV}^{nom}). The SoC of future EVs arrivals ($\widehat{SoC}_{EVs,k}^{arr}$) are estimated through the average SoC of all past EV connections. On the other hand, the total energy lost due to EV departures (E_k^{dep}) corresponds to a proportion of the average charge of all EVs. This assumption is reasonable because the EVPA algorithm, detailed in section III, assures almost equitable SoC among all EVs.

III. ELECTRIC VEHICLE POWER ALLOCATION ALGORITHM

The EVPA operates in synchronism with the TMPC and it works as a router of energy to assure that all EVs are charged up to $SoC = 80\%$ before their departure time using as much as possible renewable energy. In this paper, the

target SoC was setup as 80%, but the control architecture can operate with other values of SoC. Based on equation (13), neither EMPC nor TMPC have any information about the energy stored in each EV, but only the total energy of the entire EV parking, named E_{EV} . Due to the incomplete information about the SoC of each EV, the full charging of individual EVs cannot be guaranteed with only the Hierarchical MPC (HMPC) power assignment, especially when EVs connect at a different time or with different SoC.

To tackle this problem without raising the computation cost, HMPC operates synchronously with EVPA algorithm. This light adjunct module determines hourly the portion of EV parking power reference calculated by HMPC ($P_{EV}^{ref} = P_{EV}^{ch} + P_{EV}^{dis}$) that must be assigned to each EV. It also updates the maximum charging (P_{EV}^{maxCh}) and discharging (P_{EV}^{maxDis}) power rate of equations (7) and (8) for the next periods. The sharing of these two variables among the hierarchical control layers avoids losing performance because adjusting the power boundaries according to the real EV parking capacity prevents HMPC from charging EVs that are already fully charged or discharging EVs that are already empty.

The EVPA algorithm shares the EV parking power reference (P_{EV}^{ref}) among each plugged EVs identified by an ID number based only on three input values: the current SoC of each EV ($SoC_{EV_{ID}}$), the user's input departure time ($t_{EV_{ID}}^{dep}$), and the EV discharging authorisation ($\delta_{EV_{ID}}^{disA}$). If the EV's owner has authorised the EV's discharging, $\delta_{EV_{ID}}^{disA}$ is worth 1; otherwise, it is equal to 0.

As shown in Fig. 3, the EVPA algorithm is a recursive algorithm composed of four steps. The first step – named *Measurement* – processes the three-input data mentioned above to calculate all necessary variables for the next step. Using the user's input departure time ($t_{EV_{ID}}^{dep}$), the minimum time to charge the EV_{ID} up to $SoC_{EV_{ID}}^{max} = 80\%$ ($t_{EV_{ID}}^{minCharge}$) can be calculated through (17). This formulation considers that each EV_{ID} will be charged with its maximum charging power rate ($P_{EV_{ID}}^{maxCh}$) during the smallest sample time of HMPC, i.e. TMPC sample time ($T_s = 1h$). Similarly, the remain time in which EV_{ID} will stay connected to the BMG ($t_{EV_{ID}}^{con}$) is calculated through (18), where $t_{current}$ is the current time.

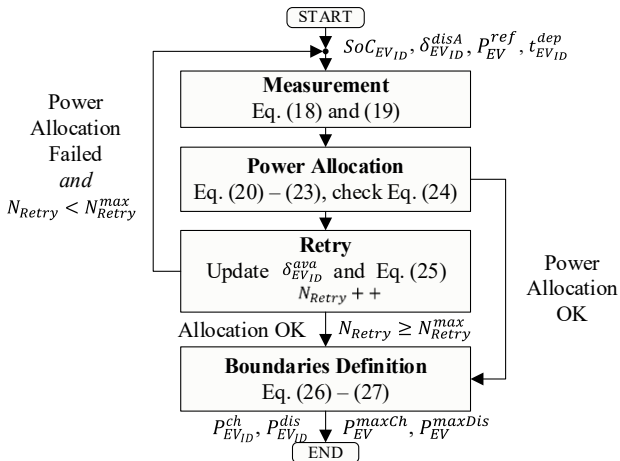


Fig. 3: Summary of the EVPA module algorithm

$$t_{EV_{ID}}^{minCharge} = \text{ceil} \left(\frac{SoC_{EV_{ID}}^{max} - SoC_{EV_{ID}}}{|P_{EV_{ID}}^{maxCh}| \cdot \frac{\eta_{ch} \cdot T_s}{v_{EV_{ID}}}} \right) \quad (17)$$

$$t_{EV_{ID}}^{con} = t_{EV_{ID}}^{dep} - t_{current} \quad (18)$$

In the second step, named *Power Allocation*, the power reference determined by HMPC ($P_{EV,k}^{ref}$) is shared among all EVs plugged at instant k following (19) if charging ($P_{EV,k}^{ch} \neq 0$), and (20) if discharging ($P_{EV,k}^{dis} \neq 0$). In these equations, ω_{ID}^{ch} and ω_{ID}^{dis} are the power-sharing weights to determine the power reference for each plugged EV ($P_{EV_{ID},k}^{ch}$ or $P_{EV_{ID},k}^{dis}$). Remarkably, the equations (19) and (20) limit the power-sharing according to the charging-discharging maximum power rate of each EV ($P_{EV_{ID}}^{maxCh}$ and $P_{EV_{ID}}^{maxDis}$). Additionally, by embedding the second term in equations (19) and (20), the EV power assignment is limited to the maximum and minimum SoC ($SoC_{EV_{ID}}^{max}$ and $SoC_{EV_{ID}}^{min}$) of each EV.

$$P_{EV_{ID}}^{ch} = \max \left(P_{EV_{ID}}^{maxCh}; \frac{SoC_{EV_{ID},k} - SoC_{EV_{ID}}^{max}}{\eta_{ch} \cdot T_s / v_{EV_{ID}}}; \omega_{ID}^{ch} \cdot P_{EV,k}^{ch} \right) \quad (19)$$

$$P_{EV_{ID}}^{dis} = \min \left(P_{EV_{ID}}^{maxDis}; \frac{SoC_{EV_{ID},k} - SoC_{EV_{ID}}^{min}}{T_s / (\eta_{dis} v_{EV_{ID}})}; \omega_{ID}^{dis} \cdot P_{EV,k}^{dis} \right) \quad (20)$$

$$\Delta t_{EV_{ID}}^{ch} = t_{EV_{ID}}^{con} - t_{EV_{ID}}^{minCharge} \quad (21)$$

$$\omega_{ID}^{dis} = \frac{\Delta t_{EV_{ID}}^{ch}}{\sum_{ID} \Delta t_{EV_{ID}}^{ch}} \cdot \delta_{EV_{ID}}^{disA} \cdot \delta_{EV_{ID}}^{ava}; \omega_{ID}^{ch} = \frac{1/\Delta t_{EV_{ID}}^{ch}}{\sum_{ID} 1/\Delta t_{EV_{ID}}^{ch}} \cdot \delta_{EV_{ID}}^{ava} \quad (22)$$

Using the margin time ($\Delta t_{EV_{ID}}^{ch}$) defined by (21), the power-sharing weights (ω_{ID}^{ch} and ω_{ID}^{dis}) are determined, as expressed in (22). The Boolean variable $\delta_{EV_{ID}}^{ava}$ is equal to 1 when the EV_{ID} is waiting for a power reference assignment, and it is equal to 0 when a power reference has already been attributed to it. Since in the first iteration, no EV received a power reference, $\delta_{EV_{ID}}^{ava}$ equals 1 for all plugged EV_{ID} . Based on equations (19), when the EV parking is charging, EV power references ($P_{EV_{ID},k}^{ch}$) will be more important for EVs that have a small margin time $\Delta t_{EV_{ID}}^{ch}$. Conversely, according to (20), when discharging, EV power references ($P_{EV_{ID},k}^{dis}$) will be more intense for EVs that have a large margin time $\Delta t_{EV_{ID}}^{ch}$.

Once determined the fraction of power that needs to be allocated to each plugged EV, the next step of the EVPA algorithm depends on the accuracy of the power-sharing weight of the previous step. As expressed in (23), if the HMPC power reference is completely allocated, the *Boundaries Definition* state is implemented; otherwise, the *Retry* state is executed. Based on equations (19) and (20), the *Retry* is executed if there would be EVs fully charged or fully discharged, or if the shared power would be limited by the power rate boundaries ($P_{EV_{ID}}^{maxCh}$ and $P_{EV_{ID}}^{maxDis}$).

$$P_{EV,k}^{ref} \neq \sum_{ID=1}^{N_{PEV}} (P_{EV_{ID},k}^{ch} + P_{EV_{ID},k}^{dis}) = \begin{cases} \text{True} \Rightarrow \text{Retry} \\ \text{False} \Rightarrow \text{Boundaries Definition} \end{cases} \quad (23)$$

Therefore, in the *Retry* state, the EVs that would be fully charged or fully discharged by applying the power reference calculated in the previous step ($P_{EV_{ID}}^{ref}$ through (19) and (20)) are identified by setting the Boolean Variable $\delta_{EV_{ID}}^{ava}$ to one, whereas all other EVs are identified to $\delta_{EV_{ID}}^{ava} = 0$.

Additionally, the power to be reallocated is the difference between the initial power reference calculated by HMPC ($P_{EV,k}^{ref}$) and the shared power that has already been well allocated, as expressed in (24). Subsequently, the *Power Allocation* step is reimplemented. This process is repeated until the condition of equation (23) is satisfied, or the number of retries surpasses a maximum threshold (N_{retry}^{max}).

$$P_{EV,k}^{ref} = P_{EV,k}^{ref} - \sum_{ID} (P_{EV_{ID}}^{ch} + P_{EV_{ID}}^{dis}) \cdot (1 - \delta_{EV_{ID}}^{ava}) \quad (24)$$

Afterwards, the fourth and last step – named *Power Boundaries Definition* – is executed. In this step, the HMPC power boundaries for EV charging and discharging (P_{EV}^{maxCh} and P_{EV}^{maxDis}) are calculated based on the estimated future SoC ($SoC_{EV_{ID},k+1}$) and the power reference calculated in the *Power Allocation* step ($P_{EV_{ID}}^{dis}$ and $P_{EV_{ID}}^{ch}$). First, the future SoC at $k + 1$ of each plugged EV is calculated through (25). Afterwards, the EV power boundaries are calculated using equations (26) and (27) and transmitted to HMPC. Remarkably, the EV power boundaries (P_{EV}^{maxCh} and P_{EV}^{maxDis}) are the sum of maximum power rate that each EV can support for the next hours.

$$SoC_{EV_{ID},k+1} = SoC_{EV,k} - P_{EV_{ID}}^{dis} \frac{T_s^{TMPC}}{v_{EV_{ID}} \eta_{dis}} - P_{EV_{ID}}^{ch} \frac{\eta_{ch} T_s^{TMPC}}{v_{EV_{ID}}} \quad (25)$$

$$P_{EV,k+1}^{maxCh} = \sum_{ID} \max \left(P_{EV_{ID}}^{min}, \frac{SoC_{EV_{ID},k+1} - SoC_{EV_{ID}}^{max}}{\eta_{ch} \cdot T_s / v_{EV_{ID}}} \right) \quad (26)$$

$$P_{EV,k+1}^{maxDis} = \sum_{ID} \min \left(P_{EV_{ID}}^{max}, \frac{SoC_{EV_{ID},k+1} - SoC_{EV_{ID}}^{min}}{T_s / (\eta_{dis} v_{EV_{ID}})} \right) \cdot \delta_{EV_{ID}}^{disA} \quad (27)$$

IV. RESULTS

To evaluate the performance of the proposed HMPC coupled with the EVPA algorithm, a real-sized residential BMG with technical specifications shown in Table 1 was simulated. The PV power generation was modelled using real solar profiles [24]. Similarly, the building's power consumption refers to a medium-sized residential building scaled from [25]. The simulations were conducted to assess three aspects: the potential of the hierarchical BEMS in maximising PV self-consumption using EV parking batteries, the impact of the size of EV parking, and the economic advantages of discharging EVs to supply the building demand. These three main points are investigated in Sections A, B and C, respectively. An additional sensitivity analysis of the electricity price is provided in Section D to consider the electricity price and EV batteries price evolution.

TABLE 1: TECHNICAL SPECIFICATION OF THE BUILDING MICROGRID.

Component	Technical Description
Photovoltaic panels	Annual energy generation: 131 MWh (100 kWc)
Building load	Annual energy consumption: 307 MWh
Li-ion batteries	Nominal capacity: 167 Ah Maximum power rate: 60 kW
EV parking (Zoe of Renault [®])	Maximum power rate: 7 kW (slow mode) Nominal capacity (Q_{EV}^{nom}): 130 Ah
Grid limit power	100 kWh

A. Performance of the hierarchical EMS

To assess the performance of the proposed controller in exploiting the EV's batteries to increase the PV self-consumption, the proposed EVPA was confronted with two types of controllers: a classical MPC in which each EV is treated independently (similar to the controller in [6]), and the

uncontrolled strategy. The uncontrolled approach charges EVs with their maximum power rate as soon as they are plugged into the BMG. On the other hand, the classical HMPC is also composed of EMPC and TMPC, but it optimises the cost function defined in (28) rather than (1). In this formulation, the self-consumption and the charging of EVs are weighted through the variable ω_k , which is higher when the EV departure is imminent (less than 3 hours from the programming departure). Since the classical HMPC does not contain the EVPA algorithm that considers the aggregation of EV park, it requires two inequality constraints (similar to equation (13)) per EV charging station.

$$\min_{SoC_{ref}^{dis}, E_{EV}^{ref}} \sum_{k=1}^{48} \frac{(|E_{grid,k}^{import}| + |E_{grid,k}^{export}|)}{\max(\max(P_{cons}^{[k,k+48]}), \max(P_{pv}^{[k,k+48]})) + \omega_k \cdot (SoC_{pev}^{target,k} - SoC_{pev,k})} \quad (28)$$

s.t.: Eq. (5) – (12) and Eq. (13) for each EV

Since the objective is to charge EV's batteries as much as possible from renewable energy, the metrics of comparison are the building self-consumption rate, coverage rate (equation (2)), and the number of EVs completed charged. Additionally, to verify the limitations on the real implementations, the execution time of each is compared.

The performance of these three control strategies was assessed under an ideal and a realistic scenario. In the ideal scenario, all EVs connect to the BMG as specified in their schedule table. Furthermore, there is no error in the power imbalance prediction data, and all EVs arrive every day with SoC=40%.

On the contrary, the realistic scenario includes inaccuracies in the power imbalance, the energy that EV batteries have stored when they plug into the BMG, and the planned departure and arrival time. The error introduced into the two day-ahead power imbalance prediction data follows equation (29), where g and Δ are calculated through equations (30) and (31), respectively. The variable ϑ is a standard Gaussian random variable of mean 0 and standard deviation 1, whereas the factor ρ is a uniformly distributed random variable in the interval of $[0, r(k)]$, where $r(k)$ is a non-linear function that depends on the instant k and it is defined as shown in the left graph in Fig. 4. Consequently, the gain g have a shape as shown in the right graph in Fig. 4. Additionally, the real prediction data is shifted in time randomly up to ten times $r(k)$, i.e. up to 6 hours. The random variable $r(k)$ was defined as shown in Fig. 4 to mimic the rising of prediction error along the MPC horizon. As a result, the error in the amplitude of the signal increases over time, detaining 0% of errors at the current time and attaining up to 60% of errors 48 hours ahead. It is important to remark that the same two day-ahead prediction data errors are introduced in both EMPC and TMPC layers. The comparison between the real and the predicted two day-ahead power imbalance at instant $k = 0$ is shown in Fig. 5.

$$P_{disturbed,k} = g \cdot P_{real,k+\Delta}, \quad \forall k \in [1,48] \quad (29)$$

$$g = 1 + \text{sign}(\vartheta) \cdot \rho_k \quad (30)$$

$$\Delta = \text{floor}(10 \cdot \rho_k \cdot \text{sign}(\vartheta)) \quad (31)$$

Additionally, the noise in the initial EV SoC follows a Gaussian distribution of a standard deviation of 5% and a mean that depends on the user behaviour. Four types of users

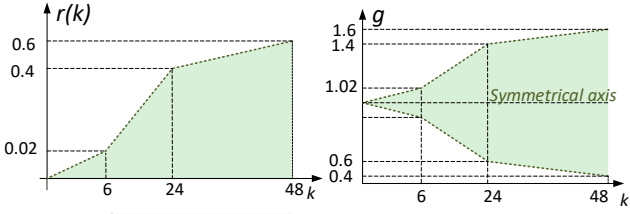


Fig. 4: Distribution of the time-variant random factors to emulate the error in the two day-ahead prediction data.

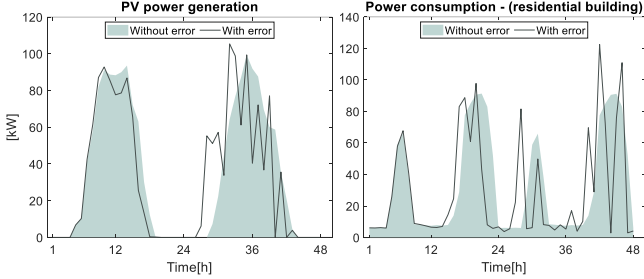


Fig. 5: Prediction data with and without error along the Economic Model

were considered. Consequently, four mean values were used, namely 30%, 40%, 50%, and 60. Finally, the noise in the departure and arrival times has also a Gaussian distribution around typical values bounded by a maximum variation of 4 hours.

The 30-days simulation results in Table 2 show that the proposed hierarchical MPC coupled with EVPA in the realistic scenario assured the self-consumption and coverage rate 7 percent point (p.p.) higher than the uncontrolled strategy. Compared to the classical HMPC, the proposed HMPC coupled with EVPA can assure a self-consumption and a coverage rate up to 1 p.p. higher.

Thanks to the periodic optimisations of TMPC and of EMPC explained in section II, the classical and the proposed HMPC proved robust against power imbalance prediction data, reducing by only 1 p.p. the annual self-consumption. Compared to the classical HMPC, the proposed one demonstrated more robustness because it could also keep the same values of coverage rate, while the classical one reduced it by 2 p.p.

Furthermore, Fig. 6 shows that both classical HMPC and HMPC with EVPA can guarantee that all EVs are charged closed to the target SoC (i.e. 80%). However, the HMPC coupled with EVPA could charge all EVs to SoC over 79%, while the classical HMPC charged some EVs to only 76%. This is because the classical HMPC depends on weight factors in the cost function (variable ω in equation (28)), while the proposed HMPC guarantees the EV charging by changing an inequalities constraint (equation (14)). According to Table 2, even though the uncontrolled approach charged all EVs to SoC=80%, less than 3% were provided by PVs, compared to more than 12% with the proposed EVPA

and 6% with the classical HMPC. This result highlights the main goal and main interest of the proposed control structure: the algorithm manages to increase radically the self-consumption of the building while maintaining a satisfying SoC of the EVs at departure time.

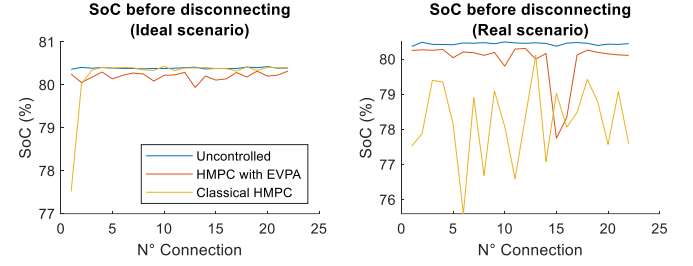


Fig. 6: Distribution of the state-of-charge of four electric vehicles just before disconnecting from the building microgrid.

With the aim of verifying the differences in the charging and discharging of ESSs when employing each control strategy, the power flow during three sample days were analysed (Fig. 7). By convention, in the graphs in Fig. 7, the charging of ESSs is negative, while the discharging is positive. Additionally, the raw net power imbalance is the difference between the power consumption and the PV power generation. Therefore, it is negative when there is energy surplus, and positive otherwise. Therefore, to reduce the grid energy exchange, it is necessary to charge the Li-ion batteries and EVs preferably when there is energy surplus (negative raw energy imbalance). In the opposite case, ESSs should be discharged to supply the building energy deficit (positive raw energy imbalance). Consequently, to maximise the coverage and self-consumption rates, it is needed to maximize the overlap of raw energy imbalance and the energy bars of ESSs.

Following this reasoning, the power flow shown in Fig. 7b and Fig. 7c for the realistic scenario proves that the classical HMPC and the HMPC with EVPA charge and discharge EV's batteries to avoid energy injection and to reduce electricity purchase, contrary to the uncontrolled strategy in Fig. 7a. Furthermore, both control strategies could charge the EVs to the target SoC (SoC \geq 80%) before their departure time (SoC equals to zero.). Since the SoC of EVs shown in Fig. 7 are the SoC measurements from the point of view of the BEMS, when an EV leaves the BMG, their SoC is measured as zero.

By observing the power flow in Fig. 7, it is also possible to note that the building storage is sometimes used to charge EVs (indicated by black arrows). Particularly, the classical HMPC sometimes discharges some EVs to charge others (indicated by red arrows in Fig. 7b). However, charging an EV with energy coming from another EV is not optimal due to charging/discharging losses. Therefore, this does not result

TABLE 2: 30-DAYS SIMULATION RESULTS TO EVALUATE THE PERFORMANCE OF DIFFERENT CONTROL STRATEGIES

Metrics	Uncontrolled		HMPC with EVPA		Classical HMPC	
	Ideal ^a	Realistic ^b	Ideal ^a	Realistic ^b	Ideal ^a	Realistic ^b
Self-consumption (%)	56.6	50.7	58.6	57.8	57.3	56.4
Coverage rate (%)	40.0	36.6	43.7	43.7	41.3	43.8
Discharge EVs (%)	0.0	0.0	21.0	23.5	8.9	8.5
Charge EVs from PVs (%)	2.6	4.6	12.3	16.4	6.7	9.2
Charge EVs from building storage (%)	30.8	26.1	15.1	14.4	22.3	19.8
Charge EVs from grid (%)	66.6	69.3	51.6	45.7	62.29	62.5

Obs: Building microgrid with 4 Electric Vehicles and Li-Ion batteries; ^a Without data prediction error; ^b With data prediction error;

in better use of energy storage systems, since the self-consumption and coverage rates of classical HMPC were lower than the proposed HMPC with the EVPA. To improve the classical HMPC, it would be recommended to include additional constraints to impede the controller to charge an EV with energy coming from another EV. This will certainly increase the complexity of the HMPC design. Moreover, large number of inequality constraints and control variables requires more time to the CPLEX solver to find the best solution.

Fig. 7 also reveals that EVs can reduce grid energy exchange more actively during weekends than weekdays. This is because EVs stay plugged for longer periods, enabling the controller to discharge EVs without compromising their fully charging. Conversely, during weekdays, EVs are plugged mostly during non-business hours, which is mostly between 5 PM to 8 AM. Consequently, EVs are connected to the BMG during periods of energy deficit (positive) and disconnected from the BMG when there is an energy surplus (negative). Hence, the BMG usually must purchase electricity from the grid to charge EVs. This behaviour is the result of a poor adequation of the PV power production and the EVs' storage availability. In fact, the performance of the three algorithms studied is comparatively impacted. According to Table 2, the HMPC with EVPA can charge the EV batteries using less grid energy than the other two control strategies. However, neither strategy can charge their EVs using only renewable energy. They need to import from the external grid at least 46% of the EVs energy demand, even though the BMG has a surplus of energy (self-consumption is not 100%). Owing to the BMG sizing, the building storage is not large enough to store all PV surplus to charge EVs during the night. The percentage of charging EV with renewable energy would be more important with a larger stationary battery. However, this would drastically increase the installation cost of the BMG.

B. Impact of the size of electric vehicle size

It is important to highlight that these conclusions were drawn from the simulation of the BMG with four EVs. To verify the impact of the EV parking size, scenarios with 0, 20, and 40 EVs were also evaluated by running the BMG with the proposed HMPC with EVPA for one year. As shown in Table 3, with the enlargement of EV parking, the charging of EVs with energy coming directly from PV panels is limited to 6 MWh/year. Likewise, with more EVs, the Li-ion battery pack is discharged more frequently to charge the EV's batteries, but they are limited to discharge up to 7 MWh/year. For this reason, the total energy imported from the main grid

TABLE 3: ONE-YEAR SIMULATIONS WITH A DIFFERENT NUMBER OF ELECTRIC VEHICLES USING THE HIERARCHICAL MPC WITH EVPA.

Metrics	0 EV ^b	4 EV ^b	20 EV ^b	40 EV ^b
Self-consumption (%)	69	71	72	72
Coverage rate (%)	29	30	28	25
Grid energy import ^a	217	234	314	416
Grid energy injection ^a	41	38	37	37
Energy to charge EVs ^a	0	27	127	249
- from grid ^a	0	19	114	237
- from PV panels ^a	0	4	6	6
- from batteries ^a	0	4	7	6
Energy discharged from EVs ^a	0	5.4	18.3	32.7

^a Annual values in MWh

^bWith Li-ion batteries

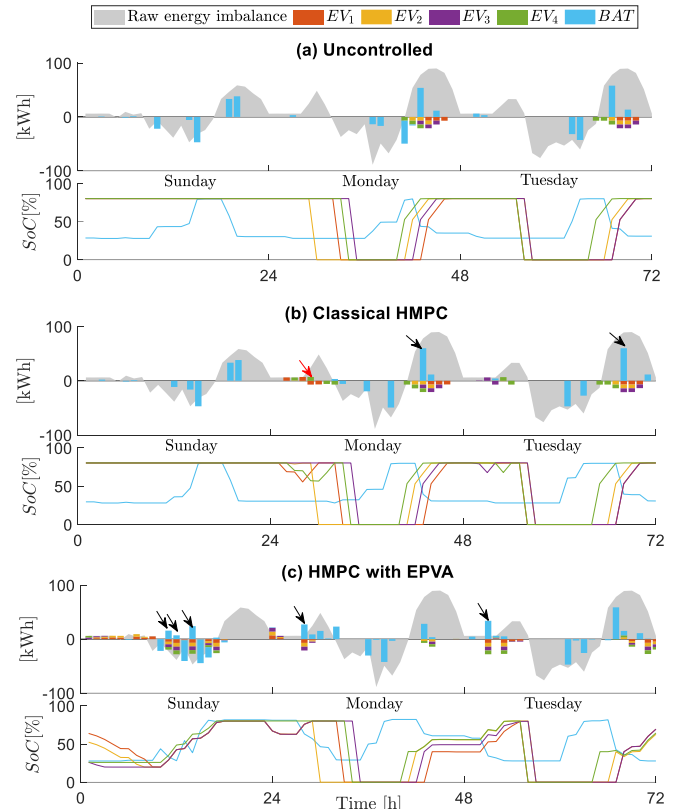


Fig. 7: Sample days of the power flow with the three control strategies with 4 electric vehicles with data prediction errors.

tends to increase, and the coverage rate tends to decrease with the enlargement of EV parking. Following the same reasoning, the self-consumption rate can be increased by up to 3 p.p. compared to the case with only batteries (column "0 EV"), but it is limited to around 72%. These results reveal that there is an optimal number of EVs that a BMG can have connected to increase the annual self-consumption rate without reducing drastically the coverage rate.

This saturation is due to the raw net power imbalance and the connection profile of EVs disposal. To increase the charging of EVs from renewable energy, the total energy used to charge PEVs in each daily connection must be matched by the daily surplus of energy. However, as shown in , depending on the raw net power imbalance, complete EV load matching is impossible.

To highlight the effects of the EV park size in the algorithm computation cost, the execution time of the EMPC optimization when using the classical HMPC architecture and the proposed HMPC with EVPA were compared. The execution time of the two methods were measured using an Intel Core i5-6200U CPU at 2.30 GHz. According to Fig. 9, the execution time of the classical HMPC rises exponentially with the number of EVs, while the EVPA keeps a similar algorithm complexity independently of the number of EV charging stations. This result indicates that the proposed HMPC with EVPA can be adapted to larger scales of applications, potentially plug-and-play, without any heavy modification of the hardware specifications, at least when it comes to computational power.

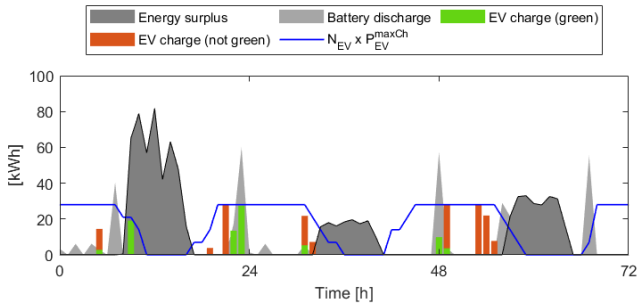


Fig. 8: Visualisation of the effects of the disposal of raw net power imbalance and the connection profile of plug-in vehicles on the charging of electric vehicles batteries with renewable energy.

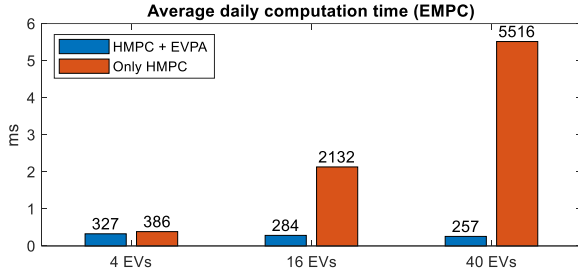


Fig. 9: Comparison of execution time when employing or not the EVPA.

C. Technical-economic analysis of discharging electric vehicles' batteries

To evaluate the economic advantages of discharging EV batteries to support the BMG energy needs, the case where 4 EVs can be discharged was compared to the case where they cannot be discharged. These two scenarios were also confronted with the case where only batteries are installed (named '0 EV') to verify the consequences of having or not EV parking. The graphs in Fig. 10 show some metrics obtained after a one-year simulation, including the battery degradation, the additional income offered by the French government, self-consumption rate, coverage rate, and electricity cost.

The battery degradation cost considers a capital cost of 500 €/kWh [26] with end-of-life when it loses 20% of its nominal capacity [27]. The battery capacity loss was estimated using the model of a Li-ion battery that exists in the SimPowerSystem library in Matlab Simulink. This model considers the current intensity, the depth of discharge, and temperature to emulate the battery capacity loss [28].

On the other hand, the additional income is calculated based on the French energy policy [29] to financially encourage self-consumption in small prosumers. This policy is based on a reward-penalty mechanism to favour the internal load match and avoid grid energy injection. It

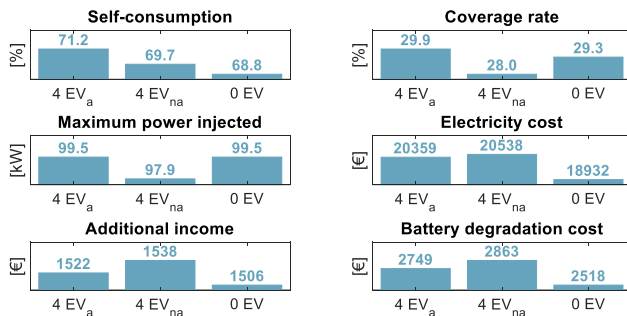


Fig. 10: Key performance indicators when four EVs are allowed (4 EV_a) and not allowed (4 EV_{na}) to be discharged, and when no EV exists (0 EV).

provides a higher additional income for small annual maximum power injected and an elevated annual self-consumption rate.

According to the results shown in Fig. 10, from the point of view of the BMG, the discharging of EVs implies a reduction in the annual electricity bill of 179 €/year. In this study, a time-of-used tariff of 0.09 €/kWh was used. Although the annual self-consumption rate was higher when allowing the EV discharging, the additional income was lower due to the increase in the maximum power injection. By comparing the degradation cost of batteries, the discharging of EV parking reduces the use of the building batteries pack, decreasing its degradation cost by 114 €/year. This is because the load shaving implemented by stationary batteries is partially covered by EV charging and discharging.

Therefore, the total savings when allowing the EV discharging – being equal to the sum of electricity (C_{elec}) and battery degradation costs (C_{elec}) minus the additional income (C_{sc}) (equation (32)) – are 282 €/year. Compared to the total BMG expenses (more than 21587 €/year), these savings are minimal. Due to the power imbalance profile, EV schedule time and sizing of the battery pack, EVs can be rarely discharged. According to Table 1 and Table 3, EV discharging represents less than 2% of annual building energy consumption for 4 EVs.

$$Total\ cost = C_{elec} + C_{bat} - C_{sc} \quad (32)$$

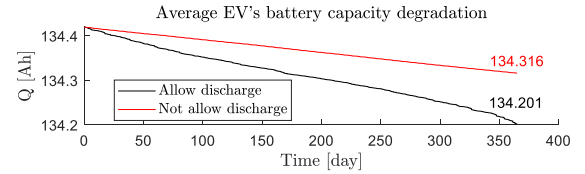


Fig. 11: Comparison of the level of degradation of batteries when electric vehicles are allowed and not allowed to be discharged.

From the perspective of the EV's owners, the discharging of their EV's batteries increases the degradation rate of EV's batteries. As shown in Fig. 11, the average capacity of EV's batteries (Q) at the end of the year is smaller when allowing discharging them than not allowing it. According to the website of Renault, the current price of batteries of Renault Zoe® costs on average 8100 € depending on the country. Taking this value to estimate the equivalent cost of discharging the EV's batteries, the additional loss of batteries' capacity of 115 mAh/year means 34.57 €/year (or 0.025 €/kWh) for each EV's owner.

Considering the hypothesis that the BMG would refund the degradation provoked by the additional degradation cost of EV batteries, the BMG profit would be only about 143.72 €/year. Therefore, the differences between both sides when allowing or not discharging EV batteries are small compared to the annual building expenses. From the perspective of EV users, discharging their EV batteries may be a disadvantage because their batteries would be degraded faster than in normal operating conditions without contributing substantially to the performance of the BMG or the use of renewable energy. Fig. 10 also illustrates that having EV parking installed in the BMG increases the electricity expenses on average of 1516.50 €/year. This is because, despite all, EVs are still a load that consumes energy. With the sizing of the BMG and the connection profile of EVs, the

BMG must purchase electricity to charge its EVs, which increases the total electricity costs by 8%.

D. Electricity price sensitivity study

To extrapolate the study to other scenarios, a sensitivity analysis on the electricity price and EV battery cost was conducted. Knowing that the EV discharging is profitable, if the additional EV battery degradation cost provoked by the discharging is less than the total BMG cost (equation (32)), it is possible to define the condition of profitability (equation (33)). Since the objective is to evaluate the impact of electricity price and EV battery cost variations on the BMG profitability, these two terms are multiplied by an unknown factor, namely α_{elec} for the electricity price and α_{EV} for the EV battery cost.

$$\alpha_{EV} \cdot (C_{elec}^a - C_{elec}^{na}) < \alpha_{elec} \cdot (C_{elec}^a - C_{elec}^{na}) + (C_{bat}^a - C_{elec}^{na}) - (C_{sc}^a - C_{sc}^{na}) \quad (33)$$

To better visualize the condition of profitability, Fig. 12 shows the combination of the gain in the electricity price and gain in the EV batteries cost that makes discharging EV batteries advantageous. As concluded previously, the EV discharging is profitable, but it is not attractive due to the low margin of benefit. However, as shown in Fig. 12, if the electricity price increases and the EV batteries decreases, the discharging can be more economically advantageous.

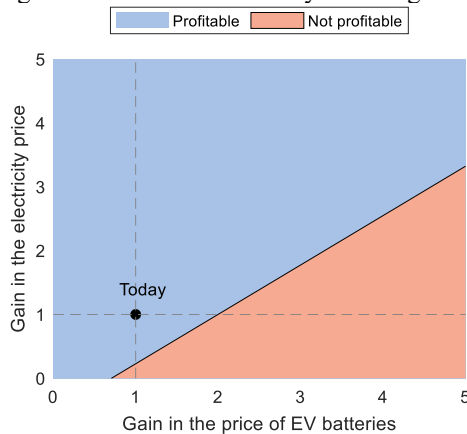


Fig. 12: Economic analysis of the electricity price and EV battery cost to verify the profitability of discharging EVs batteries.

V. CONCLUSION

The proposed hierarchical control structure has proved effective in fully charging EVs before their departure time while promoting PV self-consumption. The proposed BEMS increased up to 7 percent point the annual self-consumption compared to the uncontrolled strategy, and up to 1 percent point than the classical HMPC. Besides reducing the execution time compared to the classical HMPC, the EVPA guaranteed EV's state-of-charge over 78% even when subjected to data prediction inaccuracies. Nonetheless, due to the raw net power imbalance, sizing of battery packs, and the daily connection and disconnection profiles of electric vehicles, the charging of electric vehicles from renewable energy (6 MWh from batteries and 6 MWh from PVs) is saturated to 9% of annual photovoltaic energy generation (131 MWh/year). Consequently, with the enlargement of EV parking, the annual self-consumption rate is saturated to 72%. Electric vehicle parking also results in a considerable

increase in electricity expenses, increasing the purchased energy by about 8% of the annual building consumption with 4 EVs, and 91% with 40 EVs. Additionally, the economic advantages of discharging EVs to promote self-consumption represents only 1.3% of the annual building expenses. From the point of view of EV's owners, the monetary reward may not be enough to encourage them to authorise the discharge since their batteries would be degraded faster without substantial impact on the use of renewables. However, the economic sensitivity analysis indicates that the increase in the electricity price and the reduction of EV batteries cost could make the EV discharge more attractive. These results have to be mitigated by the choice of the case of study.

As future work, the estimation of the number of plugged EVs could be improved by analysing the user daily behaviour. This would improve the flexibility of the whole hierarchical controller since the users would not need to schedule their arrival and departure time. Additionally, it is needed to extrapolate the analysis conducted in simulation to real systems. Further investigation is required to deal with possible concerns related to communication latency, limitations in the computation resources, noise measurements, and resilience against faults. It is therefore vital that future research considers all the economic and technical peculiarities of real applications to make possible the integration of renewable energy sources in the building environment in the foreseeable future. More specifically, future works will focus on the installation of photovoltaic panels, batteries and electric vehicle in the ESTIA's building. This adequation of the storage availability and the renewable energy source production appears crucial when deciding if a building will profit from EV charging stations installation. The results presented in this article are to be implemented on a real building microgrid using hardware in the loop tools, with special care given to each of the comparison points depicted in this article.

VI. ACKNOWLEDGEMENT

The authors would like to thank New Aquitaine Region (Agreement: AAPFO424953) for their financial support.

VII. REFERENCES

- [1] International Energy Agency, "Global EV Outlook 2020 - prospects for electrification in transport in the coming decade," Technology report, Jun. 2020.
- [2] M. Muratori *et al.*, "The rise of electric vehicles—2020 status and future expectations," *Prog. Energy*, vol. 3, no. 2, p. 022002, Apr. 2021, doi: 10.1088/2516-1083/abe0ad.
- [3] Y. Zheng, "Integrating plug-in electric vehicles into power grids: A comprehensive review on power interaction mode, scheduling methodology and mathematical foundation," *Renewable and Sustainable Energy Reviews*, p. 16, 2019.
- [4] J. A. Sanguesa, V. Torres-Sanz, P. Garrido, F. J. Martinez, and J. M. Marquez-Barja, "A Review on Electric Vehicles: Technologies and Challenges," *Smart Cities*, vol. 4, no. 1, pp. 372–404, Mar. 2021, doi: 10.3390/smartcities4010022.
- [5] M. Gilleran *et al.*, "Impact of electric vehicle charging on the power demand of retail buildings," *Advances in Applied Energy*, vol. 4, p. 100062, Nov. 2021, doi: 10.1016/j.adapen.2021.100062.
- [6] P. R. C. Mendes, "Energy management of an experimental microgrid coupled to a V2G system," *Journal of Power Sources*, p. 12, 2016.
- [7] M. Tavakoli, F. Shokridehaki, M. Marzband, R. Godina, and E. Pouresmaeil, "A two stage hierarchical control approach for the optimal energy management in commercial building microgrids based on local wind power and PEVs," *Sustainable Cities and Society*, vol. 41, pp. 332–340, Aug. 2018, doi: 10.1016/j.scs.2018.05.035.

- [8] M. van der Kam and W. van Sark, "Smart charging of electric vehicles with photovoltaic power and vehicle-to-grid technology in a microgrid; a case study," *Applied Energy*, p. 11, 2015.
- [9] G. Barone, A. Buonomano, C. Forzano, G. F. Giuzio, and A. Palombo, "Increasing self-consumption of renewable energy through the Building to Vehicle to Building approach applied to multiple users connected in a virtual micro-grid," *Renewable Energy*, vol. 159, pp. 1165–1176, Oct. 2020, doi: 10.1016/j.renene.2020.05.101.
- [10] A. Buonomano, "Building to Vehicle to Building concept: A comprehensive parametric and sensitivity analysis for decision making aims," *Applied Energy*, vol. 261, p. 114077, Mar. 2020, doi: 10.1016/j.apenergy.2019.114077.
- [11] D. Borge-Diez, D. Icaza, E. Açikkalp, and H. Amaris, "Combined vehicle to building (V2B) and vehicle to home (V2H) strategy to increase electric vehicle market share," *Energy*, vol. 237, p. 121608, Dec. 2021, doi: 10.1016/j.energy.2021.121608.
- [12] S. Verma *et al.*, "A comprehensive review on energy storage in hybrid electric vehicle," *Journal of Traffic and Transportation Engineering (English Edition)*, vol. 8, no. 5, pp. 621–637, Oct. 2021, doi: 10.1016/j.jtte.2021.09.001.
- [13] Y. Zhou, S. Cao, and J. L. M. Hensen, "An energy paradigm transition framework from negative towards positive district energy sharing networks—Battery cycling aging, advanced battery management strategies, flexible vehicles-to-buildings interactions, uncertainty and sensitivity analysis," *Applied Energy*, vol. 288, p. 116606, Apr. 2021, doi: 10.1016/j.apenergy.2021.116606.
- [14] X. Jin *et al.*, "Hierarchical Management for Building Microgrid Considering Virtual Storage System and Plug-in Electric Vehicles," *Energy Procedia*, vol. 103, pp. 219–224, Dec. 2016, doi: 10.1016/j.egypro.2016.11.276.
- [15] R. Lamedica, S. Teodori, G. Carbone, and E. Santini, "An energy management software for smart buildings with V2G and BESS," *Sustainable Cities and Society*, vol. 19, pp. 173–183, Dec. 2015, doi: 10.1016/j.scs.2015.08.003.
- [16] G. K. Farinis and F. D. Kanellos, "Integrated energy management system for Microgrids of building prosumers," *Electric Power Systems Research*, vol. 198, p. 107357, Sep. 2021, doi: 10.1016/j.epsr.2021.107357.
- [17] Y. Wu, Z. Wang, Y. Huangfu, A. Ravey, D. Chrenko, and F. Gao, "Hierarchical Operation of Electric Vehicle Charging Station in Smart Grid Integration Applications — An Overview," *International Journal of Electrical Power & Energy Systems*, vol. 139, p. 108005, Jul. 2022, doi: 10.1016/j.ijepes.2022.108005.
- [18] C. Wu, S. Jiang, S. Gao, Y. Liu, and H. Han, "Charging demand forecasting of electric vehicles considering uncertainties in a microgrid," *Energy*, vol. 247, p. 123475, May 2022, doi: 10.1016/j.energy.2022.123475.
- [19] N. Liu, Q. Chen, P. Li, J. Lei, and J. Zhang, "A Heuristic Operation Strategy for Commercial Building Microgrids Containing EVs and PV System," *IEEE TRANSACTIONS ON INDUSTRIAL ELECTRONICS*, vol. 62, no. 4, p. 11, 2015.
- [20] D. Y. Yamashita, I. Vechiu, and J.-P. Gaubert, "Hierarchical Coordination of a Vehicle-to-Grid System to Improve Self-consumption in Building MicroGrids," in *2021 International Conference on Smart Energy Systems and Technologies (SEST)*, Vaasa, Finland, Sep. 2021, pp. 1–6. doi: 10.1109/SEST50973.2021.9543333.
- [21] O. Ouramdane, E. Elbouchikhi, Y. Amirat, and E. S. Gooya, "Optimal sizing of domestic grid-connected microgrid maximizing self consumption and battery lifespan," *IFAC-PapersOnLine*, vol. 55, no. 12, pp. 683–688, Jan. 2022, doi: 10.1016/j.ifacol.2022.07.391.
- [22] Enedis l'électricité en réseau, "Conditions de raccordement des Installations de stockage." Oct. 2017.
- [23] Y.-W. Chung, B. Khaki, T. Li, C. Chu, and R. Gadh, "Ensemble machine learning-based algorithm for electric vehicle user behavior prediction," *Applied Energy*, vol. 254, p. 113732, Nov. 2019, doi: 10.1016/j.apenergy.2019.113732.
- [24] "JRC Photovoltaic Geographical Information System (PVGIS) - European Commission." https://re.jrc.ec.europa.eu/pvg_tools/en/tools.html#MR (accessed Mar. 05, 2020).
- [25] S. Lee, D. Whaley, and W. Saman, "Electricity Demand Profile of Australian Low Energy Houses," *Energy Procedia*, vol. 62, pp. 91–100, 2014, doi: 10.1016/j.egypro.2014.12.370.
- [26] S. K. Kim, K. H. Cho, J. Y. Kim, and G. Byeon, "Field study on operational performance and economics of lithium-polymer and lead-acid battery systems for consumer load management," *Renewable and Sustainable Energy Reviews*, vol. 113, p. 109234, Oct. 2019, doi: 10.1016/j.rser.2019.06.041.
- [27] Y. Li *et al.*, "Data-driven health estimation and lifetime prediction of lithium-ion batteries: A review," *Renewable and Sustainable Energy Reviews*, vol. 113, p. 109254, Oct. 2019, doi: 10.1016/j.rser.2019.109254.
- [28] N. Omar *et al.*, "Lithium iron phosphate based battery – Assessment of the aging parameters and development of cycle life model," *Applied Energy*, vol. 113, pp. 1575–1585, Jan. 2014, doi: 10.1016/j.apenergy.2013.09.003.
- [29] Commission de Régulation de l'Énergie, "Cahier des charges de l'appel d'offres portant sur la réalisation et l'exploitation d'Installations de production d'électricité à partir d'énergies renouvelables en autoconsommation et situées en métropole continentale." Dec. 26, 2019.